Review of Scientific Instruments ARTICLE scitation.org/journal/rsi

A modified piezoelectric ultrasonic composite oscillator technique for simultaneous measurement of elastic moduli and internal frictions at varied temperature

Cite as: Rev. Sci. Instrum. 91, 015110 (2020); doi: 10.1063/1.5135360
Submitted: 6 November 2019 • Accepted: 25 December 2019 •
Published Online: 14 January 2020

Mingyu Xie[1,2] and Faxin Li[1,2,a)]

AFFILIATIONS

[1]LTCS and College of Engineering, Peking University, Beijing 100871, China
[2]Center for Applied Physics and Technology, Peking University, Beijing, China

[a)]Author to whom correspondence should be addressed: lifaxin@pku.edu.cn

ABSTRACT

In this work, a modified piezoelectric ultrasonic composite oscillator technique (M-PUCOT) is developed for measuring a material's elastic moduli and internal frictions, as a function of temperature. Different from the traditional PUCOT that employs two quartz bars as the drive and gauge, here, a single small piezoelectric transducer (PZT) ring is used to drive and sense longitudinal or torsional vibration in a cylinder specimen. Because of the strong piezoelectric effect and relatively large bandwidth of the PZTs compared to their quartz counterpart, the frequency match condition between the transducer and the specimen is not required in this M-PUCOT. For high temperature measurement, a fused quartz spacer, whose resonance frequency matches the specimen's, is bonded between the transducer and the specimen to provide thermal insulation. First, the united equivalent circuit of the transducer- (spacer) -specimen composite system was derived. Then, Young's modulus, longitudinal friction, shear modulus, and torsional friction were explicitly obtained by measuring the resonance frequency and antiresonance frequency of the 2- or 3-component system's electrical susceptance curve using an impedance analyzer. The accuracy of this method was validated both by measuring the system's amplitude-frequency curves using a laser vibrometer and through finite element simulations. The repeatability error of the M-PUCOT is only ~0.2% for moduli measurement and ~2.5% for internal friction measurement, which is very promising for studying the moduli and internal friction variations during damage, fatigue, and phase transitions. Finally, the M-PUCOT was employed to measure the variations in moduli and internal frictions of an $Fe_{64}Ni_{36}$ Invar alloy from room temperature to 500 °C. Results show that above the ferromagnetic phase transition temperature Tc, both moduli reach their maxima, and both internal frictions reach their minima. The proposed M-PUCOT is expected to be widely used in the near future for its quick measurement, high repeatability, and low cost.

I. INTRODUCTION

Elastic moduli and internal frictions are a material's fundamental properties, and their accurate and quick measurement is very important to the field of science and engineering. Generally, the experimental techniques for measuring the elastic moduli and internal frictions can be divided into four groups:[1] quasistatic, subresonance, resonance, and wave propagation. For quasistatic methods, the elastic moduli (Young's modulus E and shear modulus G) can be calculated from the slope of stress-strain curves, and internal frictions can be determined according to the area of stress-strain hysteresis loops. However, the quasistatic methods are usually not suggested as the testing errors are typically large (~10%). Subresonance techniques measure the internal frictions according to the phase lag between stress and strain. A commercial dynamic mechanical analyzer (DMA) and Kê pendulum[2] are typical representatives. The main advantage of these methods is that they can conduct experiments at different frequencies (10^{-4}–10^{2} Hz) and strain

amplitudes (10^{-6}–10^{-3}).[3] However, for materials with low internal friction (<10^{-3}), a small phase lag obscured by noise is difficult to be measured.[4] Resonance methods are currently most widely used for moduli and internal friction measurement. The free-free beam method[5] and impulse excitation technique (IET),[6,7] which measure the elastic moduli based on the flexural or torsional resonance of a rectangular bar-shaped specimen, are strongly dependent on the support location and support manner. Furthermore, the longitudinal and torsional internal frictions generally are not suggested to be measured directly as the errors in measuring the amplitude-frequency curve are fairly large because the supporting points must be at a small distance from the nodal positions.[5] The resonant ultrasound spectroscopy (RUS) method[8,9] can measure all the 21 independent elastic constants based on matching the numerically computed eigenfrequencies to the measured vibration modes. However, it is difficult for RUS to become a standard method where explicit formulas are usually required. As a noncontact method, the electromagnetic acoustic resonance (EMAR) method[10,11] can not only measure the anisotropic elastic constants but also measure the internal frictions corresponding to different resonance modes. The problem of EMAR is that it only applies to metals and a very high power (~kW) is required to drive the EMATs. As to the wave propagation methods,[12] elastic moduli and internal frictions can be measured according to the time of flight and decay of wave amplitudes.[13,14] However, the errors for moduli measurement by wave propagation methods are typically larger than those by resonance methods. Furthermore, the wave dispersion in the specimen and the reflection on the boundary may lead to the overestimation of the true attenuation.[4]

It should be noted that it is difficult for the abovementioned methods to measure the elastic moduli (E and G) and the related internal frictions simultaneously, accurately, and quickly, which is a practical requirement in many fields. The piezoelectric ultrasonic composite oscillator technique (PUCOT)[15–18] has been claimed to accomplish these tasks perfectly. Furthermore, temperature dependent elastic moduli and internal friction measurement can easily be accomplished by the PUCOT.[19–22] However, the traditional PUCOT has not been widely used for modulus measurement.[15–17]

The PUCOT has been developed by quite a few investigators. In 1925, Quimby[23] made a theoretical analysis of the longitudinal vibration of a bar with the arbitrary length driven by a quartz crystal oscillator. The resonance frequency and the end velocity were measured to obtain the internal friction. Based on Quimby's theory, Zacharias[24] proposed that Young's modulus of the specimen can be obtained according to the admittance curve through an iterative algorithm. However, the exact expression of internal friction cannot be obtained. In the 1950s, Marx added a second quartz crystal to the resonant system acting as a strain gauge.[16] Three frequency-matching components (the drive quartz, gauge quartz, and specimen match their resonance frequencies within 3%) were cemented together, and an AC voltage V_d was applied to the drive quartz. By measuring the voltage V_g across the gauge, the internal friction (Q^{-1}) and the maximum strain (ε_{max}) of the specimen can be obtained. In the 1970s, Robinson[17,18] derived the correct solutions of the composite system through an LCR equivalent circuit and obtained $Q^{-1} \propto V_d/V_g$ and $\varepsilon_{max} \propto V_g$. Meanwhile, the torsional and flexural quartz oscillators were proposed to measure the internal frictions in different vibration modes.[18,25,26] The PUCOT has also been used to study the amplitude-dependent internal frictions (ADIFs) as the maximum strain amplitude excited in the specimen can be from 10^{-12} to 10^{-4}.[27,28] For high or low temperature measurements, the specimen was connected to the drive-gauge assembly by a fused quartz spacer to form a 4-component system.[19–22]

The traditional PUCOT always employs quartz crystal bars to excite/receive the resonance of the 3- or 4-component system. However, because of the rather weak piezoelectricity and narrow resonance band of the quartz crystals, a frequency match between the quartz crystal bar and the specimen is required with the tolerance typically less than 3%.[16] That is, the specimen's moduli should almost be known in advance to design the quartz crystal bar. Thus, the PUCOT cannot be used to measure materials whose moduli are totally unknown. When the frequency match condition is satisfied, the PUCOT is usually used to measure the internal frictions under longitudinal, torsional, or flexural resonance modes.[17,18,25] However, the measurement of torsional friction has some problem because the torsional mode of quartz crystals is not purely torsional.[18] Due to these problems, the PUCOT has not been widely used and thus is unfamiliar to most scholars in the engineering field.

In this work, we proposed a modified piezoelectric ultrasonic composite oscillator technique (M-PUCOT) in which a single longitudinal or torsional piezoelectric transducer (PZT) ring is used to drive/sense the resonance of the composite system. Because of the very strong piezoelectricity and relatively wide band of the PZTs, the frequency match between the transducer and the specimen is not required at all, and the size of the PZT can be very small. First, the longitudinal and torsional PZTs as well as the composite system were introduced. Then, united equivalent circuits for longitudinal and torsional vibration of the system were derived. Young's modulus, shear modulus, and the related internal frictions were obtained explicitly from the resonance and antiresonance frequency of the system's electrical susceptance curve using an impedance analyzer. The validity of the model was confirmed both by vibration amplitude measurement using a laser vibrometer and through finite element simulations. The measurement repeatability was also tested. Finally, the M-PUCOT was used to measure the moduli and internal frictions of an $Fe_{64}Ni_{36}$ Invar alloy from room temperature to 500 °C. The proposed M-PUCOT is expected to be widely used in the near future.

II. PIEZOELECTRIC TRANSDUCER AND M-PUCOT SYSTEMS

A. PZTs for longitudinal and torsional vibration

A traditional PUCOT uses a α-quartz crystal oscillator to excite longitudinal or torsional vibration. As the background damping of the quartz oscillator is extremely small (~10^{-6}) and usually negligible, it is possible to measure a specimen with very low internal frictions (~10^{-5}).[15] However, the rather weak piezoelectricity of the quartz oscillator makes it necessary to work at the resonance frequency to excite a detectable strain in the specimen, which requires the resonance frequency of a specimen matching that of the quartz crystal oscillator. In addition, the scarcity of large quartz crystals limits the minimum testing frequency to about 30 kHz. Moreover, the quartz torsion oscillator is not a good torsional

transducer since its properties are not uniform along the circumferential direction.[18,26]

Compared with quartz crystal oscillators, the electromechanical coupling of PZT ceramics is very strong; thus, frequency matching is not required, and a small PZT can excite a large strain in the specimen. Meanwhile, a small PZT can work far below its resonance frequency, and its internal frictions can be neglected in the whole system. Moreover, both longitudinal PZTs and torsional PZTs[29] are very easy to fabricate, and their properties can be controlled to be very uniform.

Here, we employed thickness-poled PZT rings (with an outer diameter D, inner diameter d, and thickness h) to excite longitudinal or torsional vibration. For the longitudinal transducer, the PZT ring is in a conventional d_{33} mode, as shown in Fig. 1(a). For the torsional transducer, as shown in Fig. 1(b),[29] first, the thickness-poled PZT ring is cut into two half-rings; then, lateral electrodes are sprayed on the cutting faces of the two half-rings; finally, the two half-rings are bonded together using conductive epoxy with the poling directions opposite to each other. In this way, a circumferential field is applied, and a perfect torsional transducer is assembled.

B. The M-PUCOT systems

The M-PUCOT system for room temperature measurement of moduli and internal frictions is shown in Fig. 1(c), where the PZT is perfectly bonded onto a cylindrical specimen with the diameter equal to the outer diameter of the transducer. In this way, the longitudinal or torsional vibration can be excited in the transducer-specimen 2-component system with an alternating electric field applied in the axial direction or circumferential direction. For low-temperature or high-temperature measurement, as shown in Fig. 1(d), a long-enough fused quartz spacer with the same diameter is inserted between the specimen and the transducer to keep the PZTs working under an acceptable temperature. In order to ensure the accuracy of measurement, the antinode of the strain wave at room temperature should be near the joint of the spacer and the specimen.

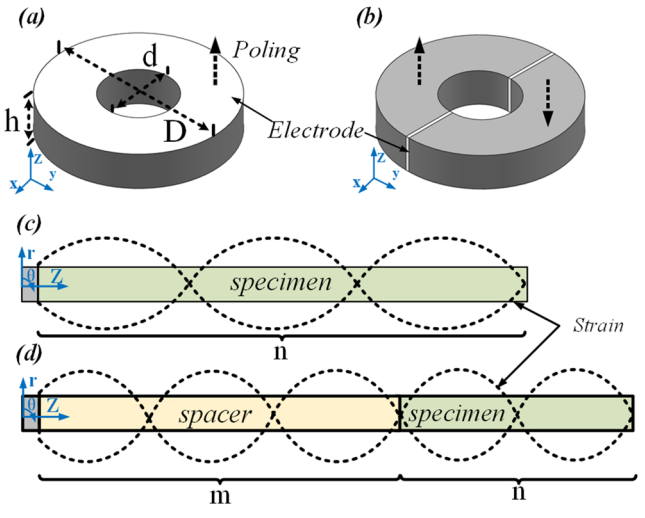

FIG. 1. PZTs and the M-PUCOT systems: (a) the thickness-mode (d_{33}) PZT, (b) the thickness-poled, thickness-shear mode (d_{15}) PZT consisting of two half-rings, (c) the transducer-specimen 2-component system for room temperature measurement, and (d) the transducer-spacer-specimen 3-component system for measurement at high or low temperature.

III. THEORY

A. Equivalent circuit model for the piezoelectric transducers

Here, we briefly derive the equivalent circuit of the longitudinal (d_{33}) mode piezoelectric transducer. As shown in Fig. 1(a), when the d_{33} piezoelectric transducer vibrates in the thickness-longitudinal mode with an oscillating electric field E_z applied parallel to its thickness, considering only the axial displacement $u_z(z,t)$, the axial strain $\varepsilon_z(z,t)$ can be expressed as

$$\varepsilon_z = \frac{\partial u_z}{\partial z}. \tag{1}$$

Taking into account the longitudinal friction(Q_{PL}^{-1}), the elastic coefficient can be written as $c_{33}^D = C_{33}'^D + jC_{33}'^D Q_{PL}^{-1}$. The one-dimensional piezoelectric constitutive equations are

$$\begin{cases} \sigma_z = c_{33}^D \varepsilon_z - h_{33} D_z, \\ E_z = -h_{33}\varepsilon_z + \beta_{33}^{\varepsilon} D_z, \end{cases} \tag{2}$$

where σ_Z and D_z are the stress and electric displacement in the axial direction, respectively, h_{33} is the piezoelectric coefficient, and β_{33}^{ε} is the constrained dielectric constant.

The equilibrium equation is

$$\frac{\partial \sigma_z}{\partial z} = \rho_P \frac{\partial^2 u_z}{\partial t^2}, \tag{3}$$

where ρ_P is the density of the PZT. By substituting σ_Z of Eq. (2) into Eq. (3) and bearing in mind that the axial electric displacement D_z is constant along the thickness, the vibration equation of the transducer can be expressed as

$$\frac{\partial^2 u_z(z,t)}{\partial t^2} = c_{PL}^2 \frac{\partial^2 u_z(z,t)}{\partial z^2}. \tag{4}$$

Note that the longitudinal wave velocity c_{PL} in the d_{33} transducer is also a complex number and c_{PL}' is the real part, given by the following equation:

$$c_{PL} = \sqrt{\frac{C_{33}^D}{\rho_P}} = c_{PL}'\left(1 + \frac{j}{2Q_{PL}}\right) = \sqrt{\frac{C_{33}'^D}{\rho_P}}\left(1 + \frac{j}{2Q_{PL}}\right). \tag{5}$$

The general solution of Eq. (4) is

$$u_z(z,t) = (A_1 \cos k_{PL} z + B_1 \sin k_{PL} z) e^{j\omega_L t}, \tag{6}$$

where ω_L is the circular frequency for longitudinal vibration and k_{PL} is the complex wavenumber whose real part determines the speed of the longitudinal wave and the imaginary part determines the attenuation of the wave amplitude, which is given by

$$k_{PL} = \frac{\omega_L}{c_{PL}} = \frac{\omega_L}{c_{PL}'}\left(1 - \frac{j}{2Q_{PL}}\right). \tag{7}$$

For the general solution in Eq. (6), the boundary conditions of velocity and force are

$$\begin{cases} \dot{u}_z|_{z=0} = U_1, \\ \dot{u}_z|_{z=h} = -U_2, \\ \int \sigma_z|_{z=0}\, dA = -F_1, \\ \int \sigma_z|_{z=h}\, dA = -F_2, \end{cases} \tag{8}$$

where U_1, F_1, U_2, and F_2 are the velocities and forces at the upper and lower faces (z = 0, h).

The electric current I in the transducer can be written as

$$I = \frac{d}{dt}\int D_z dA = j\omega_L D_z \frac{\pi(D^2 - d^2)}{4}. \tag{9}$$

From Eqs. (6), (8), and (9), we can get the transport equations of the transducer as

$$\begin{cases} F_1 = \left(\dfrac{Z_{PL}}{j\sin k_{PL}h} - \dfrac{N_L^2}{j\omega_L C_{0L}}\right)(U_1 + U_2) + Z_{PL}j\tan\dfrac{k_{PL}h}{2}U_1 + N_L V_z, \\ F_2 = \left(\dfrac{Z_{PL}}{j\sin k_{PL}h} - \dfrac{N_L^2}{j\omega_L C_{0L}}\right)(U_1 + U_2) + Z_{PL}j\tan\dfrac{k_{PL}h}{2}U_2 + N_L V_z, \\ I = -N_L U_1 - N_L U_2 + j\omega_L C_{0L} V_z, \end{cases} \tag{10}$$

where Z_{PL}, N_L, and C_{0L} are the electromechanical impedance, electromechanical conversion coefficient, and static capacitance of the d_{33} piezoelectric transducer, respectively, and $V_Z = E_z h$. The annotations and expressions for all the parameters are shown in Appendix A.

From Eq. (10), the equivalent circuit of the d_{33} mode piezoelectric transducer can be obtained, as shown in Fig. 2(a). The equivalent circuit of the torsional mode (d_{15}) piezoelectric transducer can be derived similarly,[30] and the process is not iterated here. In Fig. 2(b), the equivalent circuit of the torsional transducer is presented directly.

B. Equivalent circuit model of the M-PUCOT systems

Consider the room-temperature measurement case where a small piezoelectric transducer is directly bonded onto a cylindrical specimen, as shown in Fig. 1(c). For longitudinal vibration, according to Rayleigh's theory, the effect of lateral motion can be neglected if the length of the specimen (l_M) is much larger than the diameter (D). Thus, only axial displacement is necessary to be taken into account. Taking into account the longitudinal friction (Q_{ML}^{-1}) of the specimen, Young's modulus and the longitudinal wave velocity can be written as $E_M = E'_M + jE'_M Q_{ML}^{-1}$ and $c_{ML} = c'_{ML} + jc'_{ML}Q_{ML}^{-1}/2$, respectively, where $c'_{ML} = \sqrt{E'_M/\rho_M}$. Similarly, the transport equations of the cylindrical specimen under longitudinal vibration can be obtained as

$$\begin{cases} F_2 = -\left(Z_{ML}j\tan\dfrac{k_{ML}l_M}{2} + \dfrac{Z_{ML}}{j\sin k_{ML}l_M}\right)U_2 - \dfrac{Z_{ML}}{j\sin k_{ML}l_M}U_3, \\ F_3 = -\dfrac{Z_{ML}}{j\sin k_{ML}l_M}U_2 - \left(Z_{ML}j\tan\dfrac{k_{ML}l_M}{2} + \dfrac{Z_{ML}}{j\sin k_{ML}l_M}\right)U_3, \end{cases} \tag{11}$$

where F_2, U_2F_3, and U_3 are the forces and velocities at both ends of the specimen, i.e., $z = h$ and $h + l_M$. Z_{ML} and k_{ML} are the electromechanical impedance and complex wavenumber of the specimen for longitudinal vibration, respectively.

Based on Eqs. (10) and (11), the equivalent circuit model of the transducer-specimen composite system for longitudinal vibration can be derived straightforwardly, as shown in Fig. 3(a). A similar derivation for the torsional vibration system can be realized but not presented here. Here, we give the equivalent circuit of the torsional system directly, as shown in Fig. 3(b), and all the relevant parameters are shown in Appendix A. As to the 3-component system for measurement under varied temperature, as shown in Fig. 1(d), only the impedance of a spacer is added between the specimen and the transducer.

Taking into account the stress-free conditions at both ends of the composite system, the equivalent circuit models of the 2- or 3-component systems for longitudinal and torsional vibration can be simplified to be Figs. 3(c) and 3(d), respectively. The frequency-dependent admittances of the systems can be

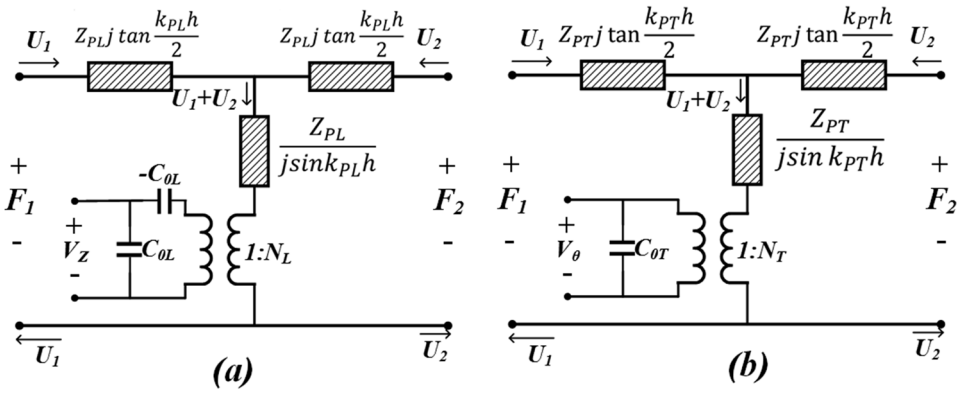

FIG. 2. The equivalent circuits of the piezoelectric transducers: (a) the longitudinal mode d_{33} transducer and (b) the torsional mode d_{15} transducer.

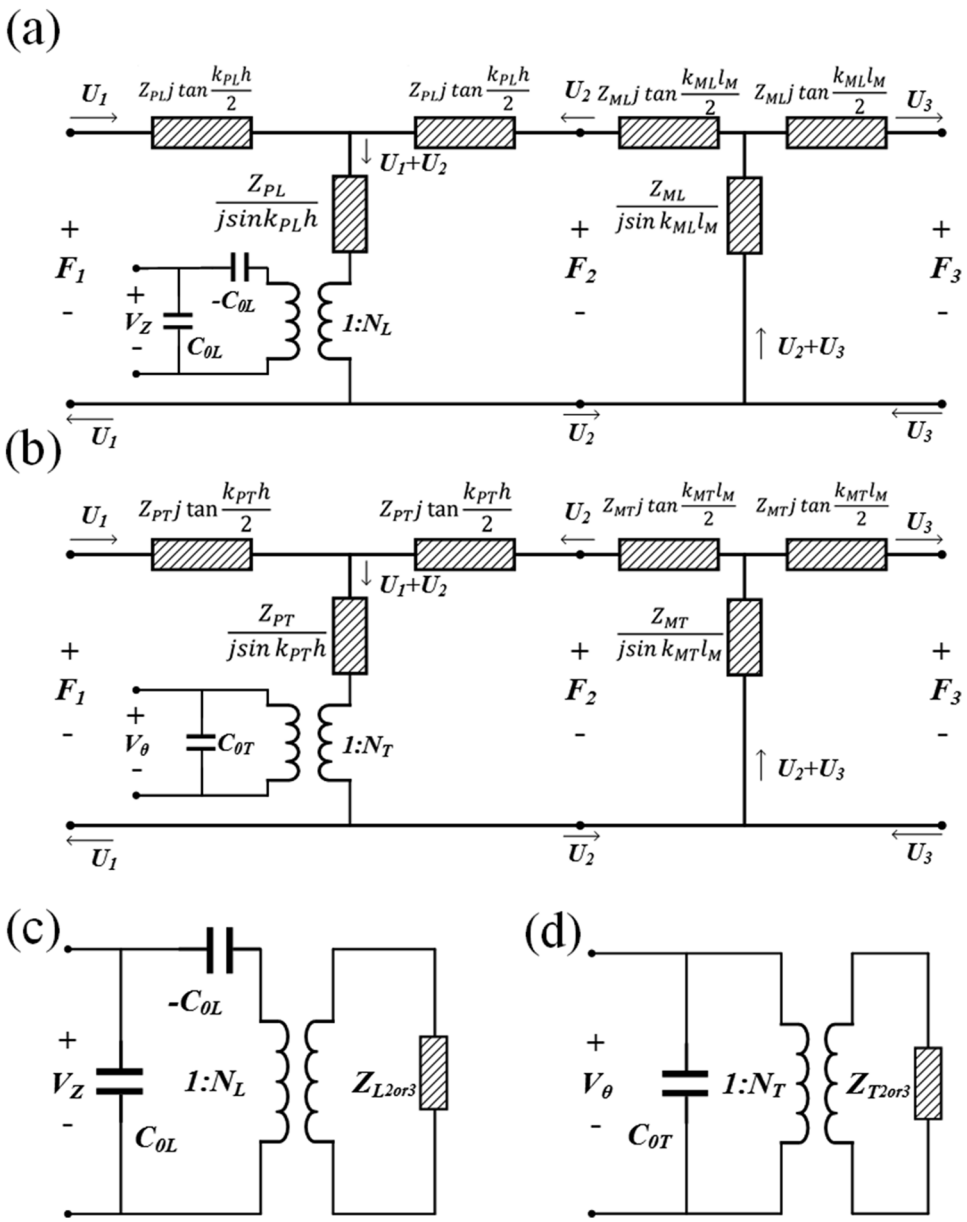

FIG. 3. The equivalent circuit of the M-PUCOT system: (a) the general case of the 2-component system for longitudinal vibration, (b) the general case of the 2-component system for torsional vibration, (c) the case with the stress-free condition at both ends of (a), and (d) the case with the stress-free condition at both ends of (b).

written as

$$\begin{cases} Y_{L_{2or3}} = jC_{0L}\omega_L + \dfrac{{N_L}^2}{-\frac{{N_L}^2}{jC_{0L}\omega_L} + Z_{L_{2or3}}}, \\ Y_{T_{2or3}} = jC_{0T}\omega_T + \dfrac{{N_T}^2}{Z_{T_{2or3}}}, \end{cases} \tag{12}$$

where $Y_{L_{2or3}}$ and $Y_{T_{2or3}}$ are the admittances of the 2- or 3-component systems for longitudinal and torsional vibration, respectively.

The electromechanical impedance of the 3-component system for longitudinal vibration can be expressed as

$$Z_{L_3} = \frac{Z_{PL}}{j\tan k_{PL}h}\frac{Z_{PL}\tan k_{PL}h + Z_{SL}\tan k_{SL}l_S + Z_{ML}\tan k_{ML}l_M}{2Z_{PL}\tan\frac{k_{PL}h}{2} + Z_{SL}\tan k_{SL}l_S + Z_{ML}\tan k_{ML}l_M}. \tag{13}$$

For the 3-component torsional vibration case, the impedance Z_{T_3} can be obtained by replacing "L" with "T" in Eq. (13).

As to the 2-component systems, the impedances for longitudinal and torsion vibrations (Z_{L_2} and Z_{T_2}) can be directly obtained by just adopting $l_S = 0$ in Eq. (13).

C. Expressions of the elastic moduli and internal frictions

As shown in Eqs. (12) and (13), the admittances of the M-PUCOT systems are complex functions of frequency, and both the real part (conduction) and the imaginary part (susceptance) can be used to calculate the elastic moduli and internal frictions of the specimen. The electrical susceptance curve (the imaginary part of admittance) is recommended to be measured because it contains the resonance points and antiresonance points which can be easily identified after flattening the slope of the curve. The purpose of flattening is to remove the slope of the curve, which only contains the transducer's information. Figure 4 shows a typical process of susceptance curve flattening. Note that for materials with very small internal frictions ($Q^{-1} < 10^{-3}$), this process can be omitted. After curve flattening, the elastic moduli and internal frictions of the specimen can be obtained by substituting the composite systems' (m + n)-order resonance frequency f^{rL}_{m+n} and antiresonance frequency f^{aL}_{m+n} into Eq. (14), where m and n are the numbers of the half-wavelength in the spacer and specimen, respectively. E_S, G_S, ρ_S, and l_S are Young's modulus, shear modulus, density, and length of the spacer, respectively. Q^{-1}_{SL} and Q^{-1}_{ST} are the longitudinal and torsional friction of the spacer, respectively, and they are so small and usually considered to be zero.

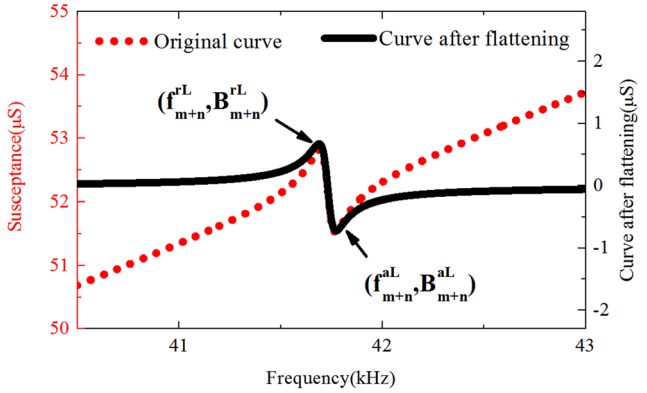

FIG. 4. Resonance and antiresonance points obtained after flattening the original susceptance curve.

$$\begin{cases} E_M = \left\{\left[1+\left(1-\dfrac{d^2}{D^2}\right)\dfrac{\rho_P h}{\rho_M l_M}+\dfrac{\rho_S l_S}{\rho_M l_M}\right]\dfrac{f^{rL}_{m+n}+f^{aL}_{m+n}}{2}2l_M-\dfrac{m\sqrt{E_S\rho_S}}{\rho_M}\right\}^2\dfrac{\rho_M}{n^2}, \\ G_M = \left\{\left[1+\left(1-\dfrac{d^4}{D^4}\right)\dfrac{\rho_P h}{\rho_M l_M}+\dfrac{\rho_S l_S}{\rho_M l_M}\right]\dfrac{f^{rT}_{m+n}+f^{aT}_{m+n}}{2}2l_M-\dfrac{m\sqrt{G_S\rho_S}}{\rho_M}\right\}^2\dfrac{\rho_M}{n^2}, \\ Q^{-1}_{ML} = 2\dfrac{f^{aL}_{m+n}-f^{rL}_{m+n}}{f^{aL}_{m+n}+f^{rL}_{m+n}}\left(1+\dfrac{m\sqrt{E_S\rho_S}}{n\sqrt{E_M\rho_M}}\right)-\dfrac{m\sqrt{E_S\rho_S}}{n\sqrt{E_M\rho_M}}Q^{-1}_{SL}, \\ Q^{-1}_{MT} = 2\dfrac{f^{aT}_{m+n}-f^{rT}_{m+n}}{f^{aT}_{m+n}+f^{rT}_{m+n}}\left(1+\dfrac{m\sqrt{G_S\rho_S}}{n\sqrt{G_M\rho_M}}\right)-\dfrac{m\sqrt{G_S\rho_S}}{n\sqrt{G_M\rho_M}}Q^{-1}_{ST}. \end{cases} \tag{14}$$

Usually, for the 3-component systems (measurement at high or low temperature), n = 1 is used. For the 2-component systems (measurement at room temperature), by substituting $l_S = 0$ and m = 0 in Eq. (14), can be significantly simplified to be the following equation. In addition, the absolute admittance (current) is almost the same as the susceptance[31] and can be used when susceptance is difficult to be measured. The error caused by this substitution can be neglected when the internal friction is large than 10^{-4}.

$$\begin{cases} E_M = \left\{\left[1+\left(1-\dfrac{d^2}{D^2}\right)\dfrac{\rho_P h}{\rho_M l_M}\right]\dfrac{f^{rL}_n+f^{aL}_n}{2}2l_M\right\}^2\dfrac{\rho_M}{n^2}, \\ G_M = \left\{\left[1+\left(1-\dfrac{d^4}{D^4}\right)\dfrac{\rho_P h}{\rho_M l_M}\right]\dfrac{f^{rT}_n+f^{aT}_n}{2}2l_M\right\}^2\dfrac{\rho_M}{n^2}, \\ Q^{-1}_{ML} = 2\dfrac{f^{aL}_n-f^{rL}_n}{f^{aL}_n+f^{rL}_n}, \\ Q^{-1}_{MT} = 2\dfrac{f^{aT}_n-f^{rT}_n}{f^{aT}_n+f^{rT}_n}. \end{cases} \tag{15}$$

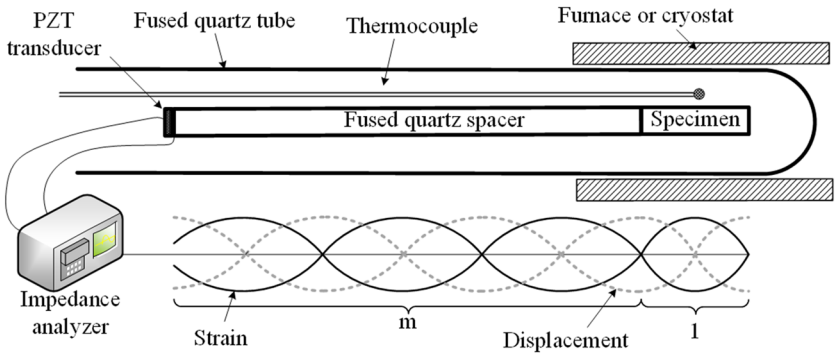

FIG. 5. The experimental setup for elastic moduli and internal friction measurement at high or low temperature.

IV. EXPERIMENTAL

A. Experimental technique

For measurement of elastic moduli and internal frictions at room temperature, the fundamental resonance (n = 1) of the transducer-specimen 2-component system is usually employed. However, for very long specimens, the fundamental resonance may not be visible, and higher-order resonances (n > 1) are suggested. The 502-epoxy cement is used to bond the PZT onto the specimen. The thin joint can act as the insulation layer for testing metallic samples, and the 502 cement can be readily removed by immersing it in acetone. A vacuum apparatus is used to reduce the impact of the external energy loses, when a "lossless" material's internal friction is required to be measured (internal friction less than 10^{-4}).

For measurement at high or low temperatures, a long fused quartz spacer is inserted between the specimen and the transducer to keep the PZTs working at an acceptable temperature, as shown in Fig. 5. In order to ensure the accuracy of internal friction measurement, the antinode of the strain wave at room temperature is required to pass through the joint of the spacer and the specimen. Actually, errors from the frequency mismatching between spacer and specimen may ordinarily be tolerated (errors for elastic modulus and internal friction can be less than 0.2% and 2% when the frequency mismatch is within 15%). The specimen at the end of the composite system is inserted into a furnace or cryostat which provides a relatively homogeneous temperature. The influence of the temperature gradient in the intermediate fused quartz spacer usually can be neglected because the internal frictions ($\sim 10^{-6}$) and frequency change (<0.3%) are very small, below 700 °C.[16,17] The temperature is conventionally controlled by a thermocouple placed near the specimen. The 502 cement is also used between the PZT and the spacer. However, due to the mismatch in the thermal expansion coefficient, the choice of bonding between the fused quartz spacer and the specimen becomes the major experimental difficulty. Here, the high-temperature cement SL8308 is employed. Other recipes can be found in the literature for both low[32,33] and high temperature[20,21] measurement.

In order to ensure the accuracy of measurement, the length of the specimen should not be very short ($\frac{l_M}{h} > 20$). Transducers are recommended to be fabricated using "hard" PZT ceramics due to their relatively small internal frictions (about 0.001–0.002). Although the supporting condition of the 2- or 3-component systems has almost no effect on the measured elastic moduli, it has a considerable effect on the measured internal frictions (especially for the "lossless" material). According to the literature,[7,16,34] thin wires or knife-edges are suggested to suspend or support the composite system near the strain wave's node. A high-resolution impedance analyzer (HIOKI IM3570, Japan) was used to measure the electrical susceptance curve of the composite system in several seconds and extract the resonance frequency and antiresonance frequency, with which the elastic moduli and internal frictions of the specimen can be calculated, based on Eq. (14).

B. Experimental results

1. Parameters of the specimen and the transducer

In this paper, the elastic moduli and internal frictions of the $Fe_{64}Ni_{36}$ Invar alloy were measured both at room temperature and from 30 °C to 500 °C using 2- and 3-component systems, respectively. The chemical compositions of the alloy are shown in Table I. For the 2-component system, the dimensions of the specimen is Φ10 mm × 80 mm. For the 3-component systems, the dimensions are Φ10 mm × 60 mm for longitudinal vibration and Φ10 mm × 57 mm for torsional vibration.

Both the longitudinal (d_{33}) mode piezoelectric transducers for Young's modulus and longitudinal internal friction measurement and torsional (d_{15}) mode piezoelectric transducers for shear modulus and shear internal friction measurement were made from the same thickness-poled "hard" PZT rings. For the d_{33} mode ring, the electric field is applied along the thickness direction; for the d_{15} mode ring, the electric field is applied along the circumferential direction. The material parameters and sizes of the "hard" PZT rings are shown in Table II.

2. Validation of the equivalent circuit model of the M-PUCOT

Before formal testing, the equivalent circuit model of the M-PUCOT system was validated using the d_{33} mode

TABLE I. Compositions of the $Fe_{64}Ni_{36}$ Invar alloy.

%	Ni	Fe	Cr	C	Mn	Si	Co	P	S
Minimum	35				0.3				
Maximum	37	rest	0.2	0.03	0.6	0.2	0.5	0.02	0.01

TABLE II. Material parameters and sizes of the "hard" PZT rings.

$D * d * h$	ρ_P	Q_{PL}^{-1} and Q_{PT}^{-1}	Curie temperature
10.0 mm * 5.0 mm * 2.0 mm	7500 kg m^{-3}	0.001–0.002	~328 °C

transducer-specimen 2-component system. First, the susceptance curve of the 2-component system was measured. Then, the 2-component system was excited using a signal generator. A laser Doppler vibrometer (Polytec VFX-l-110) was used to measure the end displacement of the system. Figure 6(a) presents the measured susceptance curve and the end displacement curve near the first mode resonance frequency. It can be seen that the peak vibration amplitude appears between the resonance frequency and antiresonance frequency of the susceptance curve. Actually, the mechanical resonance frequency f of the 2-component system is just the average value of the resonance frequency and antiresonance frequency of the electrical susceptance curve, i.e., $f = \left(f_n^{rL} + f_n^{aL}\right)/2$; In Fig. 6(a), the resonance point and antiresonance point of the susceptance curve are actually the two −3dB points around the mechanical resonance peak. Hence, the obtained formula for Q_{ML}^{-1} in Eq. (15) for the internal friction calculation is consistent with the traditional definition of internal friction, i.e., $Q^{-1} = \frac{\Delta f}{f}$.

The accuracy of Eq. (15), in which the dissipation of the transducer is neglected, was also verified by using the FEM software "COMSOL." After setting the complex Young' modulus $E_M = E_M' + jE_M'Q_{ML}^{-1}$, the resonance points and antiresonance points of the susceptance curve of the 2-component systems can be obtained in the frequency domain. The relative error between the preset value and the calculated value of Young's modulus is always within 0.1%. As shown in Fig. 6(b), the relative error of longitudinal friction measurement caused by neglecting the transducer's dissipation depends

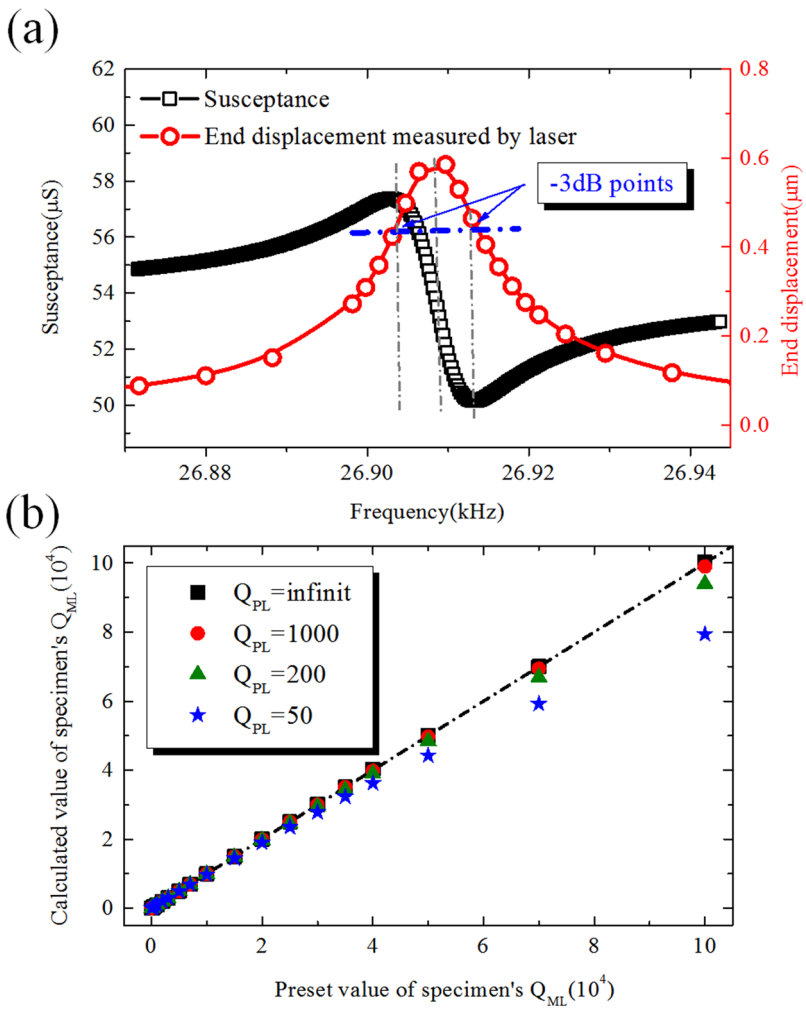

FIG. 6. Validation of the equivalent circuit model of the M-PUCOT: (a) the measured susceptance curve and end displacement curve of the d_{33} mode transducer-Invar alloy specimen system and (b) the errors of longitudinal friction measurement based on Eq. (15) using transducers with a different mechanical quality factor Q_{PL}.

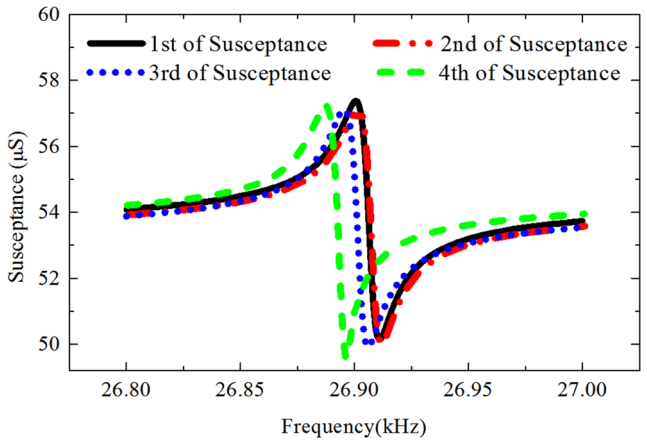

FIG. 7. Repeatability testing of the longitudinal mode 2-component system using the same cylindrical Invar alloy specimen: the 1st and 2nd testing are two *in situ* measurements using transducer A; the 3rd testing is conducted after removing transducer A and rebonding it onto the specimen; the 4th testing is conducted using transducer B with the same nominal parameters.

on both the transducer's and the specimen's Q value. A large-Q value transducer is always suggested, especially for measurement of large-Q value specimens. For example, when using a transducer with the Q value larger than 200 and the maximum tolerance error being 2.5%, the Q value range of the measurable specimen is 10–50 000, which covers most materials in practice.

Furthermore, the obtained explicit formula of the internal friction is more accurate and convenient for applications than its original definition, $Q^{-1} = \frac{\Delta f}{f}$, where Δf is usually manually obtained from the frequency response curves using the −3dB method.

3. The repeatability of the M-PUCOT

The repeatability of the M-PUCOT was further examined using the longitudinal 2-component system, and the measured susceptance curve is plotted in Fig. 7. In all the testing cases, the same cylindrical $Fe_{64}Ni_{36}$ Invar alloy was employed. The 1st and 2nd testing were conducted using the same d_{33} mode transducer, transducer A. The 3rd testing was conducted after removing transducer A and rebonding it onto the specimen. The 4th testing was conducted using another d_{33} mode transducer, transducer B. It can be seen from Fig. 7 that although different transducers with the same nominal parameters were used, the discrepancy in the measured resonance frequency is still within 0.1%, resulting in the modulus measurement error within 0.2%. Note that the longitudinal resonance frequencies of transducer A and transducer B differ about 1.5% (1.105 MHz vs 1.122 MHz) and are much larger than the resonance frequency of the specimen itself (which is about 27.3 kHz). Thus, the resonance frequency of the composite system is mainly determined by the specimen and is less dependent on the small transducer. If the same transducer is used, the repeatability error of the measured resonance frequency can be within 0.05% and that of the measured modulus can be within 0.1%. The repeatability error of the measured internal friction is larger than that of the measured modulus, which is about 1.5% when using the same transducer and about 2.5% when using different transducers. Note that the repeatable testing errors of modulus measurement using the proposed M-PUCOT are much lower than the ASTM standard methods (the free-free beam method, ASTM 1875 and impulse excitation technique, and ASTM 1876), the errors of the latter are typically about 2%.[5,6,35]

4. Measurement results at room temperature

Young's modulus (E), shear modulus (G), longitudinal friction (Q_{ML}^{-1}), and torsional friction (Q_{MT}^{-1}) of the $Fe_{64}Ni_{36}$ Invar alloy were measured at room temperature (30 °C) using the 2-component M-PUCOT system. The testing results are presented in Table III. Young's modulus measured by this method is 155.3 GPa, which fits well with the results (~152 GPa) measured by Özöğüt[36] using the impulse excitation technique (IET). The measured shear modulus is 56.4 GPa, which is consistent with the measurement results (55.3–56.1 GPa) by Decremps[37] using the wave propagation method. Nadutov[38] measured the longitudinal friction of this alloy, and the results at room temperature (~0.4×10^{-3}) agree well with the value obtained by this method (~0.41×10^{-3}). The torsional friction measured by the M-PUCOT is 0.56×10^{-3}, which is about 1.4 times the longitudinal friction. This tendency is consistent with previous measurement results on steel[39] and copper.[40] Actually, the rule that the shear friction is considerably larger than the longitudinal friction is valid for all metals. This is due to the fact that the torsional vibrations are more effective in causing dislocation movement than longitudinal vibrations,[1,40] which is thought to be the source of internal frictions in metals. This rule is also consistent with the fact that the dissipation of the torsional wave is more severe than the longitudinal wave.[41] Therefore, even when we talk about the internal friction of isotropic materials, we should indicate clearly whether it is longitudinal friction or torsional friction since the values can differ by a great extent.

5. Measurement results at high temperature

For the measurement of elastic moduli and internal frictions of $Fe_{64}Ni_{36}$ at high temperature, a fused quartz spacer (with the diameter D = 10 mm and the length l_S = 75 mm) was inserted between the specimen and transducer to keep the PZTs working at an acceptable

TABLE III. Measured parameters of the $Fe_{64}Ni_{36}$ Invar alloy cylindrical specimen at room temperature.

Length (mm)	Density (Kg/m^3)	f_1^{rL} (Hz)	f_1^{aL} (Hz)	f_1^{rT} (Hz)	f_1^{aT} (Hz)	Young's modulus (GPa)	Shear modulus (GPa)	$Q_{ML}^{-1}(10^{-3})$	$Q_{MT}^{-1}(10^{-3})$
80.0 ± 0.05	8100 ± 8.1	26 895 ± 0.1	26 906 ± 0.1	16 122 ± 0.1	16 131 ± 0.1	155.31 ± 0.31	56.41 ± 0.11	0.41 ± 0.007	0.56 ± 0.01

temperature (about 60 °C, which is much lower than the Curie temperature). The lengths of the $Fe_{64}Ni_{36}$ rods for longitudinal vibration and torsional vibration were chosen to be 60 mm and 57 mm, respectively, to ensure the antinode of the strain wave passes through the joint of the spacer and specimen at room temperature. The whole system worked in the 2-order mode, i.e., m = n = 1. 20 mm of the end of the fused quartz spacer connecting the specimen was inserted into the furnace to keep the specimen working at uniform temperatures. For all the measurements, the heating rate was fixed at 5 °C/min.

First, the elastic moduli and relative changes of internal frictions of the fused quartz spacer without bonding the specimen were measured under the same conditions (inserted 20 mm into the furnace). As shown in Fig. 8(a), the measured Young's modulus and shear modulus of the fused quartz space are 72.1 GPa and 30.9 GPa, respectively, and both are almost invariable with temperature. The absolute values of[16] and relative changes in the internal frictions of the quartz spacer are so small (~10^{-6}) that they can be neglected. Thus, Q_{SL}^{-1} and Q_{ST}^{-1} in Eq. (14) can be significantly simplified by substituting $Q_{SL}^{-1} = Q_{ST}^{-1} = 0$.

Next, the susceptance curves of the 3-component systems under different temperatures were measured using the impedance analyzer. Figure 8(b) shows the typical susceptance curves for the torsional resonance system under different temperatures. It can be seen that the average value of the resonance and antiresonance frequencies (corresponding to the shear modulus) increases first and then decreases with increasing temperature, while the "distance" between resonance and antiresonance frequencies (corresponding to torsional friction) is exactly the opposite.

The measurement results of Young's modulus and shear modulus are presented in Fig. 8(c). It can be seen that Young's modulus increases from 155.3 GPa (at 30 °C) to 168.6 GPa (at 285 °C) and then decreases to 162.6 GPa (at 500 °C). Due to the different doping amounts of Si and Cr in $Fe_{64}Ni_{36}$, the absolute value measured here is about 2% larger than that measured by Özöğüt[36] using the impulse excitation technique (IET) and Deryabin[42] using the flexural self-oscillation method. The maxima point of the Young's modulus curve is about 285 °C, which is 55 °C higher than the Curie temperature of 230 °C and is almost the same as that measured by Deryabin.[42] The measured shear modulus increases from 56.5 GPa at 30 °C to 61 GPa at 265 °C and then decreases to 57.2 GPa at 500 °C, which is between the values measured by Tanji[43] and Maeda[44] using the electrostatic driving methods. The maxima point of shear modulus measured here (about 265 °C) is lower than that measured by Young's modulus, and the same phenomenon has also been reported in previous literature studies.[43,44]

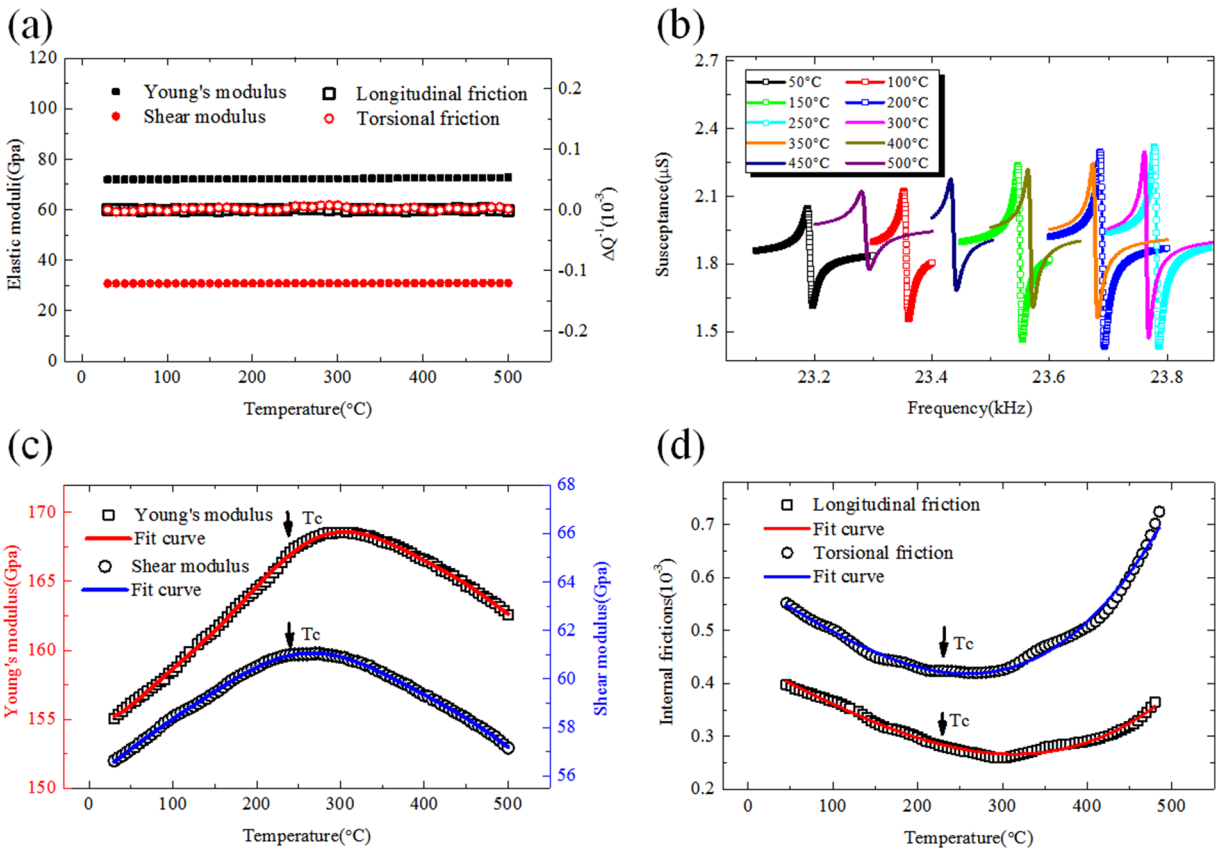

FIG. 8. The measurement results from 30 °C to 500 °C: (a) the elastic moduli and changes in internal frictions of the fused quartz spacer without the bonding specimen, (b) susceptance curves of the 3-component system for torsional vibration, (c) temperature-dependent Young's modulus and shear modulus of $Fe_{64}Ni_{36}$, and (d) temperature-dependent longitudinal friction and torsional friction of $Fe_{64}Ni_{36}$.

The measured temperature dependent longitudinal friction and torsional friction of the $Fe_{64}Ni_{36}$ Invar alloy are shown in Fig. 8(d). It can be seen that the variation tendency of the measured internal frictions with temperature is just opposite to that of the measured elastic moduli. That is, both internal frictions first decrease and then increase with increasing temperature. The minima point of the longitudinal friction curve also appears at 285 °C, coinciding with the maxima point of the Young's modulus curve, and the minima point of the torsional friction (265 °C) coincides with the maxima point of the shear modulus curve. It should be noted that the relative variation in the internal frictions (20%–40%) is much larger than that in the elastic moduli (5%–8%), so it is more advantageous to study phase transitions by measuring the internal frictions. Meanwhile, at room temperature, all the measurement results by the 3-component system are consistent with those obtained by the 2-component system, which further validates the accuracy of the 3-component system for high-temperature or low-temperature measurement.

V. DISCUSSIONS

From the abovementioned results, it can be seen that the proposed M-PUCOT can provide quick and reliable measurement of Young's modulus, shear modulus, and both internal frictions at varied temperature. Compared with the traditional PUCOT, the M-PUCOT has several unique advantages: (1) The elastic moduli and internal frictions of a specimen with unknown resonance frequency can be measured simultaneously and explicitly at room temperature, and frequency match is not required between the transducer and the specimen. (2) The piezoelectric parameters and elastic constants of the transducer do not have to be calibrated before testing. (3) Miniature PZTs are easy to fabricate and are cost-effective, which are more suitable for online measurement.

However, in order to ensure the accuracy of the M-PUCOT, the length of the specimen should not be very short ($\frac{l_M}{h} > 20$). As the thickness of transducers usually could not be less than 1 mm, the length of specimens should be more than 20 mm. Thus for tiny specimens, techniques like RUS and EMAR are more advantageous. In addition, the choice of suitable cement for high-temperature or low-temperature measurement is an experimental difficulty and strongly depends on the operator's skill.

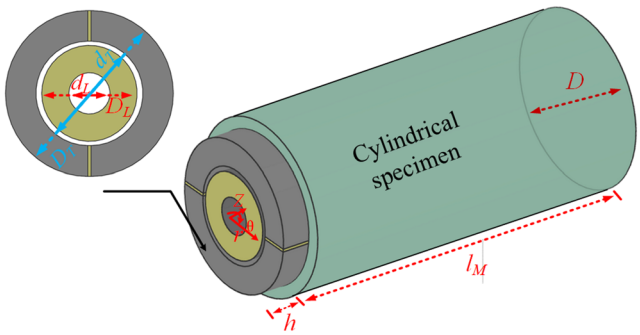

FIG. 9. Simultaneous measurement of Young's modulus, shear modulus, and both internal frictions using concentric longitudinal and torsional PZT rings.

Another issue is that in this work, we measure Young's modulus (longitudinal friction) and shear modulus (shear friction) separately using two transducers; thus, two heating/cooling cycles are required, which is inconvenient in studying phase transitions. Actually, by bonding concentric longitudinal and torsional ring transducers onto one end of the specimen (spacer), both moduli (internal frictions) can be measured simultaneously. As shown in Fig. 9, the inner diameter of the torsional transducer is slightly larger than the outer diameter of the longitudinal transducer, and both transducers have equal thickness. In this case, two impedance analyzers are required, and Eq. (15) for room temperature measurement will be slightly changed to

$$\begin{cases} E_M = \left\{\left[1+\left(\frac{D_T^2-d_T^2}{D^2}+\frac{D_L^2-d_L^2}{D^2}\right)\frac{\rho_P h}{\rho_M l_M}\right]\frac{f_n^{rL}+f_n^{aL}}{2}2l_M\right\}^2\frac{\rho_M}{n^2}, \\ G_M = \left\{\left[1+\left(\frac{D_T^4-d_T^4}{D^4}+\frac{D_L^4-d_L^4}{D^4}\right)\frac{\rho_P h}{\rho_M l_M}\right]\frac{f_n^{rT}+f_n^{aT}}{2}2l_M\right\}^2\frac{\rho_M}{n^2}, \\ Q_{ML}^{-1} = 2\frac{f_n^{aL}-f_n^{rL}}{f_n^{aL}+f_n^{rL}}, \\ Q_{MT}^{-1} = 2\frac{f_n^{aT}-f_n^{rT}}{f_n^{aT}+f_n^{rT}}, \end{cases} \tag{16}$$

where D_T and d_T are the outer diameter and inner diameter of the torsional transducer, respectively, and D_L and d_L are the outer diameter and inner diameter of the longitudinal transducer, respectively. Note that the outer diameter of the torsional transducer may not be the same as that of the specimen. Similarly, the formula for the high (low) temperature measurement system can be slightly changed accordingly, which is not presented here.

VI. CONCLUSIONS

In summary, we proposed a modified piezoelectric ultrasonic composite oscillation technique (M-PUCOT) which can measure Young's modulus and longitudinal friction and shear modulus and torsional friction explicitly, quickly, and accurately at varied temperature using a PZT ring. The repeatability error for modulus measurement is less than 0.2%, and that for internal friction measurement is within 2.5%, which are much smaller than that of the ASTM standard methods, and are more suitable for studying the phase transition process of solids. The proposed M-PUCOT overcomes several shortcomings of the traditional PUCOT and is expected to be widely used in the near future.

Actually, the maximum strain of the specimen can also be measured using the M-PUCOT, and the formula are presented in Appendix B. However, because the employed impedance analyzer can only provide very low power excitation, the induced strain is very small ($<10^{-6}$). In our ongoing work, a high-power excitation and measurement system is under development and will be implanted into the M-PUCOT. In that case, the strain amplitude dependent phenomena such as plasticity, damage, fatigue, etc.,[45,46] can be investigated by using the M-PUCOT.

ACKNOWLEDGMENTS

This work is supported by the National Natural Science Foundation of China under Grant Nos. 11672003 and 11890684.

APPENDIX A: LIST OF SYMBOLS AND NOMENCLATURES

Parameters	Expressions	Annotations
B^{rL}_{m+n} and B^{aL}_{m+n},		m + n order longitudinal resonance and antiresonance amplitude, respectively.
B^{rT}_{m+n} and B^{aT}_{m+n}		m + n order torsional resonance and antiresonance amplitude, respectively.
C_{0L} and C_{0T}	$\frac{\pi(D^2-d^2)}{4h\beta^{\varepsilon}_{33}}$ and $\frac{2h}{\pi}P^{\varepsilon}_{11}\ln(\frac{D}{d})$	Static capacitance of d_{33} and d_{15} PZTs, respectively.
C^{D}_{33}	$C'^{D}_{33}+jC'^{D}_{33}Q^{-1}_{PL}$	Elastic coefficient in open circuit of d_{33} transducer. C'^{D}_{33} is real part.
c_{ML} and c_{PL} and c_{SL}	$\sqrt{E_M/\rho_M}$ and $\sqrt{C^{D}_{33}/\rho_P}$ and $\sqrt{E_S/\rho_S}$	Longitudinal wave velocity in the specimen, d_{33} transducer, and spacer, respectively.
c_{MT} and c_{PT} and c_{ST}	$\sqrt{G_M/\rho_M}$ and $\sqrt{1/\rho_P s^{E}_{44}}$ and $\sqrt{G_S/\rho_S}$	Torsional wave velocity in the specimen, d_{15} transducer, and spacer, respectively.
D and d		The outer and inner diameter of the d_{33} and d_{15} transducers, respectively.
D_z		Electric displacement along the axial direction of d_{33} transducer.
d_{15}		Piezoelectric coefficient.
E_M and E_S	$E'_M+jE'_MQ^{-1}_{ML}$ and $E'_S+jE'_SQ^{-1}_{SL}$	Young's modulus of the specimen and spacer, respectively. E'_M and E'_S are the real parts.
E_Z		Axial electric field in the d_{33} transducers.
F_1 and F_2 and F_3		The force or moment at z = 0, h, $l_M + h$, respectively.
f^{rL}_{m+n} and f^{aL}_{m+n},		m + n order longitudinal resonance and antiresonance frequency, respectively.
f^{rT}_{m+n} and f^{aT}_{m+n}		m + n order torsional resonance and antiresonance frequency, respectively.
G_M and G_S	$G'_M+jG'_MQ^{-1}_{MT}$ and $G'_S+jG'_SQ^{-1}_{ST}$	Shear modulus of the specimen and spacer, respectively. G'_M and G'_S are the real parts.
h		The thickness of the d_{33} and d_{15} transducers.
h_{33}		Piezoelectric coefficient.
I		Electric current in the transducers.
j		$\sqrt{-1}$.
k_{ML} and k_{PL} and k_{SL}	ω_L/c_{ML} and ω_L/c_{PL} and ω_L/c_{SL}	Longitudinal wave number of the specimen, d_{33} transducer, and spacer, respectively.
k_{MT} and k_{PT} and k_{ST}	ω_T/c_{ML} and ω_T/c_{PT} and ω_L/c_{ST}	Torsional wave number of the specimen, d_{15} transducer, and spacer, respectively.
l_M and l_S		Length of the specimen and spacer, respectively.
N_L and N_T	$\frac{\pi(D^2-d^2)h_{33}}{4h\beta^{\varepsilon}_{33}}$ and $\frac{d_{15}(D^2-d^2)}{4s^{E}_{44}}$	Electromechanical conversion coefficient of the d_{33} and d_{15} transducers, respectively.
P^{ε}_{11}		Dielectric constant of the transducer.
Q^{-1}_{ML} and Q^{-1}_{PL} and Q^{-1}_{SL}		Longitudinal friction of the specimen, d_{33} transducer, and spacer, respectively.
Q^{-1}_{MT} and Q^{-1}_{PT} and Q^{-1}_{ST}		Torsional friction of the specimen, d_{15} transducer, and spacer, respectively.

APPENDIX A. (*Continued.*)

Parameters	Expressions	Annotations
S_{44}^{E}	$S_{44}'^{E} + jS_{44}'^{E}Q_{PT}^{-1}$	Elastic compliance coefficient of the d_{15} transducer. $S_{44}'^{E}$ is the real part.
u_Z		Axial displacement.
U_1 and U_2 and U_3		Velocity or angular velocity at z = 0, h, $l_M + h$, respectively.
V_z and V_θ		Axial voltage in the d_{33} transducer and circumferential voltage in the d_{15} transducer.
$Y_{L_{2or3}}$ and $Y_{T_{2or3}}$		Admittance of the 2- or 3-component system for longitudinal and torsional vibration, respectively.
Z_{ML} and Z_{PL} and Z_{SL}	$\frac{E_M \pi D^2}{4c_{ML}}$ and $\frac{\pi(D^2-d^2)c_{33}^{D}}{4c_{PL}}$ and $\frac{E_S \pi D^2}{4c_{SL}}$	Impedance of the specimen, d_{33} transducer, and spacer for longitudinal vibration, respectively.
Z_{MT} and Z_{PT} and Z_{ST}	$\frac{G_M \pi D^4}{32c_{MT}}$ and $\frac{\pi(D^4-d^4)}{32s_{44}^{E}c_{PT}}$ and $\frac{G_S \pi D^4}{32c_{SL}}$	Impedance of the specimen, d_{15} transducer, and spacer for torsional vibration, respectively.
ε_z and σ_z		Axial strain and stress, respectively.
ρ_M and ρ_P and ρ_S		The mass density of the specimen, piezoelectric transducers, and spacer, respectively.
ω_L and ω_T		Circular frequency for longitudinal and torsional vibration, respectively.
β_{33}^{ε}		Dielectric isolation constant of the d_{33} transducer.

APPENDIX B: DERIVATION OF FORMULAS FOR MODULI, INTERNAL FRICTIONS, AND MAXIMUM STRAIN BASED ON EQ. (13)

When the thickness of the PZT is much smaller than the length of the specimen, we can obtain

$$\begin{cases} \tan k_{PL}h \approx k_{PL}h + \frac{1}{3}(k_{PL}h)^3, \\ \tan k_{SL}l_S \approx k_{SL}l_S - m\pi, \\ \tan k_{ML}l_M \approx k_{ML}l_M - n\pi, \end{cases} \tag{B1}$$

where m and n are the number of half-wavelengths in the spacer and specimen, respectively. By substituting Eq. (B1) into Eq. (13), we can obtain

$$\begin{cases} Z_{L_3} \approx \frac{Z_{PL}}{jk_{PL}h}\left(1 + \frac{Z_{PL}(k_{PL}h)^3\psi_{L_3}}{4}\right), \\ \psi_{L_3} = \frac{1}{Z_{PL}k_{PL}h + Z_{SL}(k_{SL}l_S - m\pi) + Z_{ML}(k_{ML}l_M - n\pi)}, \end{cases} \tag{B2}$$

where Z_{PL}, k_{PL}, Z_{SL}, k_{SL}, Z_{ML}, and k_{ML} are complex numbers. Thus, the approximate expression of the susceptance curve of longitudinal vibration can be obtained as

$$|Y_{L_3}| \approx imag(Y_{L_3}) = \frac{\pi\left(D^2 - d^2\right)C'^D_{33}}{4h\left(\beta'^{\varepsilon}_{33}C'^D_{33} - h^2_{33}\right)}\omega_L - \frac{\left[\pi\rho_P h\left(D^2 - d^2\right)\right]^2 h^2_{33}}{64\left(\beta'^{\varepsilon}_{33}C'^D_{33} - h^2_{33}\right)^2}\mathrm{Re}(\psi_{L_3})\omega_L^4. \tag{B3}$$

As shown in Fig. 4, after flattening the susceptance curve, the resonance and antiresonance frequencies are roots of the equation: $\frac{\partial\left[(2\pi f_L)^4\mathrm{Re}(\psi_{L_3})\right]}{\partial f_L} = 0$. After simplification, the equation for f_L can be obtained: $af_L^2 + bf_L + c = 0$, and

$$\begin{cases} a = 4\pi^2\left[\frac{h\,\mathrm{Re}(Z_{PL})}{\mathrm{Re}(c_{PL})}\left(1 + \frac{Q_{PL}^{-2}}{4}\right) + \frac{l_S\,\mathrm{Re}(Z_{SL})}{\mathrm{Re}(c_{SL})}\left(1 + \frac{Q_{SL}^{-2}}{4}\right) + \frac{l_M\,\mathrm{Re}(Z_{ML})}{\mathrm{Re}(c_{ML})}\left(1 + \frac{Q_{ML}^{-2}}{4}\right)\right]^2, \\ b = -2\pi\left[m\,\mathrm{Re}(Z_{SL}) + n\,\mathrm{Re}(Z_{ML})\right]\sqrt{a}, \\ c = \pi^2\left\{\left[m\,\mathrm{Re}(Z_{SL}) + n\,\mathrm{Re}(Z_{ML})\right]^2 - \left[\frac{m\,\mathrm{Re}(Z_{SL})}{2Q_{SL}} + \frac{n\,\mathrm{Re}(Z_{ML})}{2Q_{ML}}\right]^2\right\}. \end{cases} \tag{B4}$$

Hence, we can obtain

$$\begin{cases} f^{rL}_{m+n} + f^{aL}_{m+n} = -\frac{b}{a}, \\ f^{rL}_{m+n}f^{aL}_{m+n} = \frac{c}{a}. \end{cases} \tag{B5}$$

According to Eqs. (B4) and (B5), we can obtain Eq. (14).

In addition, for the 2- or 3-component system, it can be proved that the end velocity of each component is the same. Hence, the maximum strain amplitude can be written as

$$\varepsilon_{Z\max} = \left.\frac{\partial u_{z'}}{\partial z'}\right|_{\max} = \frac{|U_2|}{c_{ML}}. \tag{B6}$$

According to Eqs. (10), (13), and (B6), we can obtain

$$\begin{cases} \varepsilon_{Z\max} = \frac{2\sqrt{2}V_Z}{\pi D}\sqrt{\frac{\left(B^{rL}_{m+n} - B^{aL}_{m+n}\right)}{\left(\frac{n\sqrt{E_M\rho_M}}{Q_{ML}} + \frac{m\sqrt{E_S\rho_S}}{Q_{SL}}\right)\frac{E_M}{\rho_M}}}, \\ \varepsilon_{\theta Z\max} = \frac{4V_\theta}{\pi D}\sqrt{\frac{\left(B^{rT}_{m+n} - B^{aT}_{m+n}\right)}{\left(\frac{n\sqrt{G_M\rho_M}}{Q_{MT}} + \frac{m\sqrt{G_S\rho_S}}{Q_{ST}}\right)\frac{G_M}{\rho_M}}}. \end{cases} \tag{B7}$$

REFERENCES

[1] M. S. Blanter, I. S. Golovin, H. Neuhauser, and H. Sinning, *Internal Friction in Metallic Materials: A Handbook* (Springer, 2010).
[2] T.-S. Kê, Phys. Rev. **72**, 41 (1947).
[3] J. Woirgard, Y. Sarrazin, and H. Chaumet, Rev. Sci. Instrum. **48**, 1322 (1977).
[4] R. S. Lakes, Rev. Sci. Instrum. **75**, 797 (2004).
[5] ASTME 1875-13, Annual Book of ASTM Standards, 2013.
[6] ASTME 1876-15, Annual Book of ASTM Standards, 2015.
[7] G. Roebben, B. Bollen, A. Brebels, J. Van Humbeeck, and O. Van der Biest, Rev. Sci. Instrum. **68**, 4511 (1997).
[8] A. Migliori, J. L. Sarrao, W. M. Visscher, T. M. Bell, M. Lei, Z. Fisk, and R. G. Leisure, Physica B **183**, 1 (1993).
[9] R. G. Leisure and F. A. Willis, J. Phys.: Condens. Matter **9**, 6001 (1997).
[10] H. Ogi, H. Ledbetter, S. Kim, and M. Hirao, J. Acoust. Soc. Am. **106**, 660 (1999).
[11] H. Ogi, M. Hirao, and T. Honda, J. Acoust. Soc. Am. **98**, 458 (1995).
[12] J. L. Rose, *Ultrasonic Waves in Solid Media* (Cambridge University Press, 1999), p. 143.
[13] S. Periyannan and K. Balasubramaniam, Rev. Sci. Instrum. **86**, 114903 (2015).
[14] M. Fukuhara and I. Yamauchi, J. Mater. Sci. **28**, 4681 (1993).
[15] R. Schaller, G. Fantozzi, and G. Gremaud, *Mechanical Spectroscopy Q−1 2001, with Applications to Materials Science* (Trans Tech Publications Inc., 2001).
[16] J. Marx, Rev. Sci. Instrum. **22**, 503 (1951).
[17] W. H. Robinson and A. Edgar, IEEE Trans. Sonics Ultrason. **21**, 98 (1974).
[18] W. H. Robinson, S. H. Carpenter, and J. L. Tallon, J. Appl. Phys. **45**, 1975 (1974).
[19] J. W. Marx and J. M. Sivertsen, J. Appl. Phys. **24**, 81 (1953).

[20]P. M. Sutton, Phys. Rev. **91**, 816 (1953).
[21]J. Weertman and E. I. Salkovitz, Acta Metall. **3**, 1 (1955).
[22]J. W. Marx, G. S. Baker, and J. M. Sivertsen, Acta Metall. **1**, 193 (1953).
[23]S. L. Quimby, Phys. Rev. **25**, 558 (1925).
[24]J. Zacharias, Phys. Rev. **44**, 116 (1933).
[25]S. D. Devine and W. H. Robinson, IEEE Trans. Ultrason., Ferroelectrics, Frequency Control **45**, 11 (1998).
[26]F. C. Rose, Phys. Rev. **49**, 50 (1936).
[27]S. Kustov, G. Gremaud, W. Benoit, S. Golyandin, K. Sapozhnikov, Y. Nishino, and S. Asano, J. Appl. Phys. **85**, 1444 (1999).
[28]S. Kustov, S. Golyandin, K. Sapozhnikov, J. Van Humbeeck, and R. De Batist, Acta Mater. **46**, 5117 (1998).
[29]Q. Huan, M. Chen, and F. Li, Ultrasonics **94**, 342 (2019).
[30]M. Xie, Q. Huan, and F. Li, e-print arXiv:1812.07784 (2018).
[31]L. Chen, F. P. Sun, and C. A. Rogers, Proc. SPIE **1917**, 286 (1993).
[32]R. B. Schwarz, Rev. Sci. Instrum. **48**, 111 (1977).
[33]T. Kosugi, Jpn. J. Appl. Phys. **33**, 2862 (1994).
[34]S. Siegel and S. L. Quimby, Phys. Rev. **49**, 663 (1936).
[35]I. Štubňa, T. Húlan, A. Trník, and L. Vozár, Acta Acust. Acust. **104**, 269 (2018).
[36]U. C. Özöğüt and A. Çakır, J. Alloys Compounds **705**, 126 (2017).
[37]F. Decremps and L. Nataf, Phys. Rev. Lett. **92**, 157204 (2004).
[38]V. Nadutov, T. Golub, and O. Hymenyuk, Funct. Mater. **11**, 497 (2004).
[39]M. Fukuhara and A. Sanpei, ISIJ Int. **33**, 508 (1993).
[40]H. Ledbetter, C. Fortunko, and P. Heyliger, J. Mater. Res. **10**, 1352 (1995).
[41]E. Leinov, M. J. Lowe, and P. Cawley, J. Sound Vib. **347**, 96 (2015).
[42]A. V. Deryabin, V. K. Kazantsev, and B. N. Shvetsov, J. Magn. Magn. Mater. **51**, 98 (1985).
[43]Y. Tanji, Y. Shirakawa, and H. Moriya, Sci. Rep. **22**, 84 (1970).
[44]T. Maeda, J. Phys. Soc. Jpn. **30**, 375 (1971).
[45]I. Golovin, H.-R. Sinning, J. Göken, and W. Riehemann, Mater. Sci. Eng. **370**, 537 (2004).
[46]W. Mason, J. Acoust. Soc. Am. **28**, 1207 (1956).